

# Ultrasound Calibration for Unique 2.5D Conical Images

Hareem Nisar<sup>a,b</sup>, John Moore<sup>a</sup>, Natasha Alves<sup>c</sup>, Germain Hwang<sup>c</sup>, Terry M. Peters<sup>a,b,d</sup>, and Elvis C.S. Chen<sup>a,b,d</sup>

<sup>a</sup>Robarts Research Institute, Canada

<sup>b</sup>School of Biomedical Engineering, Western University, Canada

<sup>c</sup>Sunnybrook Research Institute, Canada

<sup>d</sup>Department of Medical Biophysics, Western University, Canada

## ABSTRACT

Intracardiac echocardiography (ICE) systems are routinely used in percutaneous cardiac interventions for interventional and surgical navigation. Conavi's Foresight ICE is a new ICE system that uses a mechanically rotating transducer to generate a 2D conical surface image in 3D space, in contrast to the more typical side-firing phased array. When combined with magnetic tracking technology, this unique imaging geometry poses new calibration challenges and opportunities. Existing ultrasound calibration methods are designed for 2D planar images and cannot be trivially applied to unique 2.5D conical surface images provided by the Foresight ICE system. In this work a spatial and temporal calibration technique applied to the unique case of conical ultrasound image data is described and validated. Precision of calibration parameters is used to quantify the validation of our calibration method and the overall system accuracy is validated using point source and sphere centroid localization. We report a maximum error of 5.07 mm for point reconstruction accuracy and 1.94 mm for sphere centroid localization accuracy.

**Keywords:** Ultrasound calibration, intracardiac echocardiography, radial ultrasound, Conavi

## 1. INTRODUCTION

Image guidance is critical to percutaneous cardiac interventions because of the absence of the direct line of sight. Ultrasound imaging systems are suitable for cardiac imaging due to their safety, relatively low cost, high soft tissue contrast and compatibility with surgical tools. Transthoracic and transesophageal ultrasound imaging are capable of providing high contrast 2D and 3D imaging of soft tissues in real-time, but they are constrained in their views as they are used from outside the heart. In contrast, intracardiac echocardiography (ICE) is often used to guide these minimally invasive cardiac procedures by advancing the probe inside the heart and providing real-time imaging of the heart anatomy.<sup>1</sup> Conventional ICE images are 2D, planar and limited in their resolution and field of view. The recently introduced Foresight ICE system<sup>2</sup> (Conavi Medical, North York, Canada) overcomes these challenges by generating high-resolution 3D ultrasound volumes in approximately one second. The Foresight ICE probe acquires ultrasound data in spherical coordinates using a single-element mechanically rotating transducer which rotates along the azimuthal angle  $\theta$  at a specific polar angle or imaging angle  $\phi$  to generate a hollow cone shaped image (Fig. 1). Each image frame acquired by the Foresight ICE is a 2D conical surface image in 3D volumetric space. Therefore, we refer to this unique image configuration as 2.5D. Foresight ICE is also capable of generating 3D volume images by acquiring multiple 2.5D cone shaped images at varying imaging angles. Color Doppler imaging can also be obtained for side viewing images ( $\phi \geq 70^\circ$ ). These 2.5D images offer new opportunities for improving existing ICE guidance as well as potentially new clinical applications.

Ultrasound-based image guidance systems typically employ tracked tools and a tracked imaging probe. The use of electromagnetic tracking with ultrasound imaging facilitates the registration between patient anatomy, ultrasound images and other imaging modalities such as preoperative CT and MRI, and even electrophysiology

---

Send correspondence to H.N/E.C.C.

H.N.: hnisar3@uwo.ca

E.C.C.: chene@robarts.ca

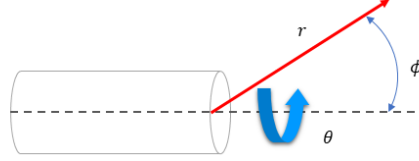


Figure 1: Scanning method for Foresight ICE probe - a single element, mechanically rotating transducer acquires data along the radial vector in a spherical coordinate system

maps to guide atrial ablation procedures. Tracking also simplifies the navigation of catheters towards a surgical target, generating 3D models using volume stitching, and visualization of compound 3D volumes from 2D images. Tracking is achieved using position and orientation (pose) sensors attached to the imaging probe. The tracking system generates a transformation between the sensor attached to an ultrasound device and the reference/world coordinate system, but the pose of the ultrasound image with respect to this reference coordinate system is unknown. Therefore, ultrasound calibration is required to determine the transformation between the coordinate system of the image volume and the sensor attached to the probe. The overall accuracy of an image-guidance system is dependent on the accuracy of this calibration as well as the accuracy of tracking system, the dimensions of the pose sensors, and the quality of imaging. However, only calibration can be controlled and improved to minimize errors in the overall system. Many calibration techniques have been described in the literature for ultrasound probes.<sup>3</sup> Ultrasound probe calibration methods for 2D planar ICE probes have been described and evaluated to provide image guidance during interventional procedures such as left atrial ablation therapy.<sup>4</sup> However, all such calibration methods are designed for 2D planar ultrasound images. The Foresight ICE system, being unique in its image acquisition technique and 2.5D conical images, has not yet included methods for tracking and calibration in the commercially available version of the technology.

In this paper, we present and evaluate an intracardiac ultrasound spatial and temporal calibration method designed for 2.5D conical ICE. Line-phantom based methods are used to perform calibrations of the ultrasound probe. We validate these calibrations by quantifying precision at different imaging angles, and the overall system by localizing a point source and computing the centroid of a sphere object.

## 2. METHODS

In all our experiments, tracking is achieved using an electromagnetic tracking system (Aurora, NDI, Canada).<sup>5</sup> The Conavi Hummingbird console along with a Foresight ICE probe is used to generate ultrasound images. Since we do not have access to the voxelized 3D data of the 2.5D conical images, we acquire the images using a frame-grabber (DVI2USB 3.0, Epiphan Video, USA). An additional step is required to convert the fiducial points from the coordinates of a planar 2D image to that of 3D space in which the ultrasound is acquired. Eqn. 1 is used to represent the relationship between the two image coordinate systems.

$$\begin{bmatrix} x_{3D} \\ y_{3D} \\ z_{3D} \end{bmatrix} = \begin{bmatrix} 1 & 0 & -o_x \\ 0 & 1 & -o_y \\ 0 & 0 & \|(x_{2D}, y_{2D})\| \cdot \tan(90 - \phi) \end{bmatrix} \begin{bmatrix} x_{2D} \\ y_{2D} \\ 1 \end{bmatrix} \quad (1)$$

where  $(o_x, o_y)$  represents the center of the planar image or the apex of the conical image.

Both the magnetic tracking system and the frame-grabber are connected to the PC using PLUS<sup>6</sup> library and the time-stamped data are imported to 3D Slicer.<sup>7</sup>

### 2.1 Calibration

Owing to the unique 2.5D conical configuration of the images acquired by the Foresight ICE system, standard cross-wire phantoms or Z-fiducial phantoms<sup>3</sup> cannot be used as they are designed for conventional 2D planar images. For the same reason, popular temporal calibration techniques and modules like fCal<sup>6</sup> cannot be used directly with 2.5D conical images. Therefore we use needle-based methods described by Chen et al.<sup>8</sup> and Gobbi et al.<sup>9</sup> for spatial and temporal calibration respectively.

### 2.1.1 Spatial Calibration

We formulate ultrasound probe calibration as a registration problem between a point and homologous line,<sup>10</sup> using a tracked needle (a line) and its hyperechoic reflection in ultrasound image (a point) as the basis for calibration. While the Foresight ICE generates a conical ultrasound image in real time, it is displayed on a conventional 2D monitor as a disc-shaped image in a 2D polar coordinate system (Fig. 2a). Given the imaging depth  $r$  and the imaging angle  $\phi$ , the 2D pixel location in the original disc image can be converted to a 3D coordinate system as per Eqn.1. In this manner, the point-line based calibration<sup>10</sup> is directly applicable to the Foresight ICE probe calibration, where efficient solutions exist.<sup>8</sup>

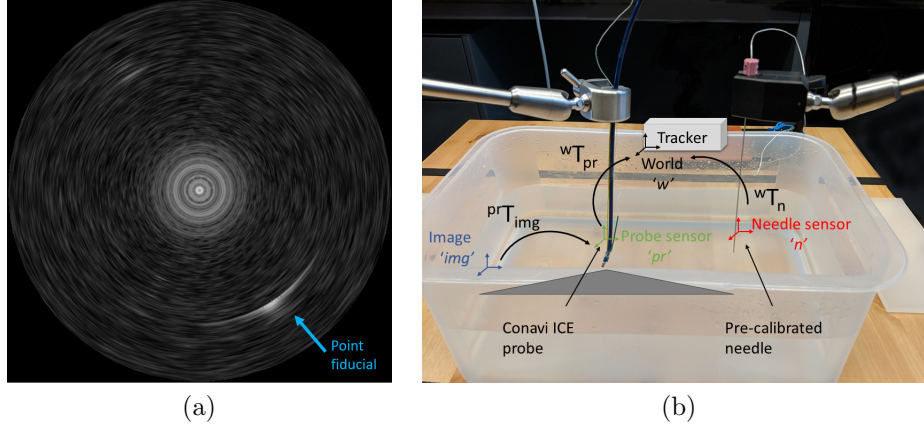


Figure 2: (a) Screen capture of Foresight ICE image as seen on the Hummingbird console and (b) experimental set up for data acquisition. Arrow shows the reflection of the needle as seen in the ultrasound image.

A Foresight ICE probe was augmented with a 6 DoF magnetic tracking sensor rigidly attached to the outer sheath, close to the probe tip. A water bath was scanned at room temperature using tracked a Foresight ICE probe. A pre-calibrated needle (Aurora Needle, 18G/150 mm, NDI, Canada)<sup>11</sup> was used to model a line. The pose of the needle is defined by a point of origin and a direction vector. The needle was oriented at multiple positions and angles to produce point fiducials on the cone shaped 2.5D images, along the radius and at varying azimuthal angles  $\theta$ . For this initial assessment, the imaging angle  $\phi$  was kept constant at 80°. Clamps were used to minimize jitter and overcome inaccuracies caused by temporal misalignment. 15 point fiducials were recorded using screen-capture of the Conavi console, along with the tracking information for both the probe and the needle. Fiducial points from the 2D images were converted using Eqn. 1 to their correct representation in 3D space.

The coordinate systems are represented in Fig. 2b, with that defined by the magnetic tracking system being considered as the world coordinate system. Let  $w$ ,  $n$ ,  $pr$  and  $img$  represent coordinate systems as defined by the tracker, needle sensor, ICE probe sensor and ultrasound image volume, respectively. As the needle is pre-calibrated, the transform  $P_1$  from needle tip to the sensor on the needle is known. The pose of the line fiducials can be defined in coordinate system of the ultrasound probe using:

$$P_2 = {}^{pr}T_{img} = ({}^wT_{pr})^{-1}({}^wT_n)P_1 \quad (2)$$

where  ${}^wT_{pr}$  and  ${}^wT_n$  are the locations of the probe sensor and needle respectively, as reported by the magnetic tracking system. Fiducial point coordinates in 3D space and pose information of the line fiducials ( $P_2$ ) are used to solve for the affine calibration transformation comprising of anisotropic scaling, followed by rotation and translation.

### 2.1.2 Temporal Calibration

We use a temporal calibration method described by Gobbi et al.<sup>9</sup> and extend it to work for the 2.5D images. This approach compares the positions of a tracked, line-shaped object in real space to those of the reflection of that object as seen in a B-mode ultrasound images. We use a 4 mm wooden shaft to represent a line and its

reflection is seen as a point in the ultrasound image. Wood is used to reduce the amplitude of the reflection at the shaft-water interface. The line is kept almost perpendicular to the 2.5D imaging plane to obtain a bright and well-defined reflection in the ultrasound image. A 6 DoF magnetic tracking sensor is rigidly attached to the shaft representing the line to track its motion. Accuracy of this method is highly dependent on the linear motion of the line with respect to the ultrasound image. To ensure smooth and unidirectional motion of the line-object, we fashioned a simple, plastic building-block assembly which moved along the tracks at the bottom of the water bath. The Foresight ICE probe remained static at one position. The block assembly carrying the wooden line-object is moved forward and backward along the tracks to generate a sinusoidal motion pattern. Reflections in the image appear in and out of the imaging angle accordingly. Five measurements were taken with imaging angle fixed at 85°. For every measurement, at least 2 motion cycles were recorded.

Segmentation of the line reflection from the images was performed automatically using 3D Slicer. The centroid of each segmented reflection from the images was extended to 3D space using Eqn. 1. The distance of this point from the origin  $O$  of the conical image is recorded to represent the positional information of the object in the image ( $img_{dist}$ ). To obtain the positional information of the line-object in real space ( $obj_{pos}$ ), the tracking sensor data were analyzed to find the linear direction of motion using Principal Component Analysis<sup>12</sup> and record the projection of sensor position along the principal axis. The two signals representing position of the object in space ( $obj_{pos}$ ) and its reflection in the image ( $img_{dist}$ ) were normalized by subtracting the mean followed by division by the standard deviation in a signal. Finally, the temporal offset was calculated by finding the time delay which provides the highest cross-correlation between the two signals.

## 2.2 Validation

We validated our calibration both qualitatively and quantitatively. Qualitative assessment was performed by generating a model of the needle used for spatial calibration and displaying its intersection with the 2.5D ultrasound image in a virtual reality environment.

We validated our calibration system by evaluating the precision of spatial calibration parameters and time offset as computed by the temporal calibration. To validate the overall system accuracy, two experiments were performed: point source localization and calculation of the centroid of a spherical object. We designed a phantom which can be used to model both the point source and a sphere object and compare the point and centroid location with pre-experiment reference positions defined by the CT scan of the phantom.

### 2.2.1 Calibration Precision

Conventionally calibration precision is evaluated at multiple depths and frequencies. Variability of parameters, as calibration is performed at different depths and frequencies, is extensively discussed in literature.<sup>3</sup> Since Foresight ICE has the functionality of adjustable imaging angle  $\phi$  of the cone shaped image, we intended to observe the trends in variability, if any. We repeat our spatial and temporal calibration experiment at multiple imaging angles to evaluate the precision of spatial calibration matrix parameters: translation along Cartesian axes, Euler rotation angles and scaling along Cartesian axes as well as the time delay observed via temporal calibration.

For spatial calibration, in all the experiments the probe was physically held in place using a clamp and the imaging angle  $\phi$  was changed through the buttons on the console. Automatic segmentation was performed using 3D Slicer to locate the needle point fiducial in the 2D images. The remainder of the procedure was as described in section 2.1.1. Similarly for temporal calibration, the experiment was repeated multiple times at three different imaging angles; keeping the probe still and only changing the imaging angle through the console.

### 2.2.2 Point Source Localization

A 140 mm by 140 mm plate phantom was designed with 4 pillars in each corner, one in the middle and 7 divots. The divots help define the reference coordinate frame via point-point registration of divot locations from tracker coordinate system to CT coordinate system. The corner pillars secure the wires going across and intersecting at one point, which is considered as the target point source (Fig. 3). The wires were roughened near the intersection to improve their echogenicity. The cross-wire phantom was scanned using the calibrated Foresight ICE probe to image the point source. A 5 mm thick layer of silicone was poured into the bottom of the phantom to help

reduce reflections. Care was taken to position the probe such that the point fiducial lies in the middle of the cone shaped image along the radius, in order to minimize the beam profile effect and associated errors. Points are converted to 3D space using Eqn. 1 followed by calibration transformation and conversion to reference coordinate system defined by the CT scanner. The ground truth is established by the point location in the 3D CT scan. Point reconstruction accuracy is described in terms of standard error and 95% confidence interval along  $x$ ,  $y$  and  $z$  axis.

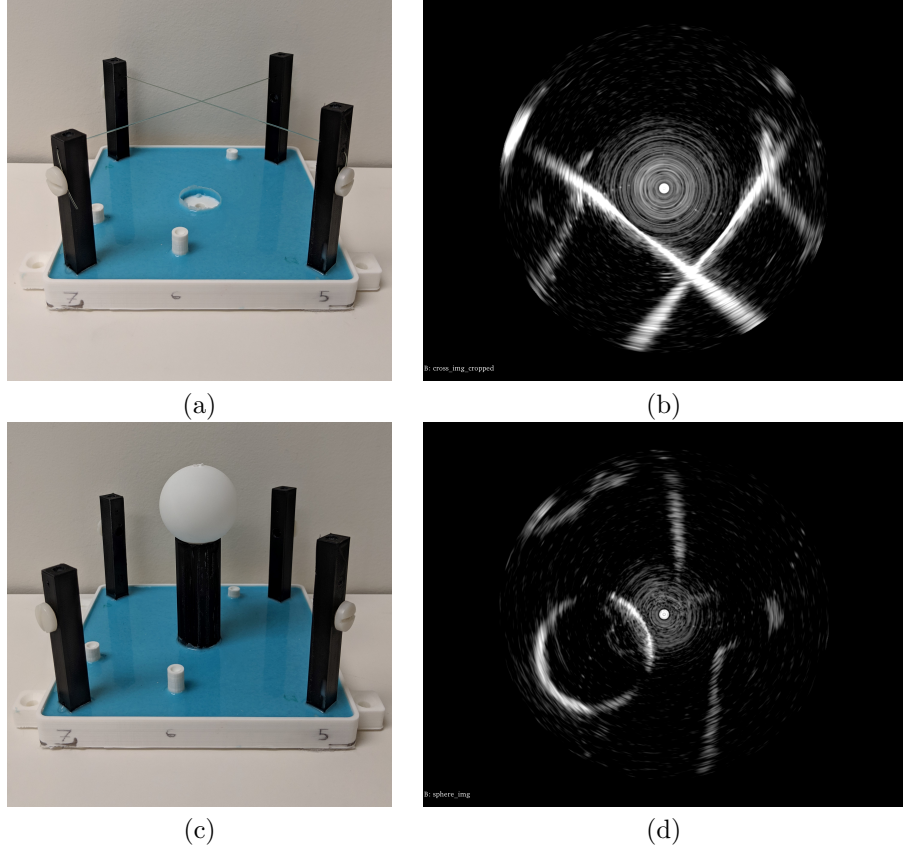


Figure 3: Validation phantom: (a) cross wire to model a point source, (b) as seen in 2.5D ultrasound and (c) sphere ball, (d) as seen in 2.5D ultrasound.

### 2.2.3 Spherical Phantom Centroid

The same phantom was adjusted to remove wires and add a 30 mm radius table-tennis ball to model a sphere. The phantom was imaged at multiple poses to identify points along the outline of the sphere at different cross-sections (Fig. 3). Then, similar to the point source localization method, the points were transformed to the reference coordinate system. Spherical fitting was applied to these points to find the center and radius of the sphere. These centroids of the sphere were compared to the one estimated in the reference coordinate system.

## 3. RESULTS

### 3.1 Calibration

#### 3.1.1 Spatial Calibration

Spatial calibration of a fixed-angle Foresight ICE probe, with a magnetic sensor attached to the outer sheath, was performed using a needle phantom and point to line registration algorithm. Results depict an overall calibration accuracy (fiducial registration error, or FRE) of 1.74 mm.

### 3.1.2 Temporal Calibration

The tracked long wooden line was moved in and out of the conical 2.5D surface plane of the Foresight ICE probe fixed at an angle of 85°. Correlation was used to find a temporal offset between the two sinusoidal signals: position of line in 3D space ( $obj_{pos}$ ) and distance of point reflection from the center of the image ( $img_{dist}$ ). A time delay of 72 ms was observed in this experiment. Figure 4 shows the normalized signals before and after temporal calibration.

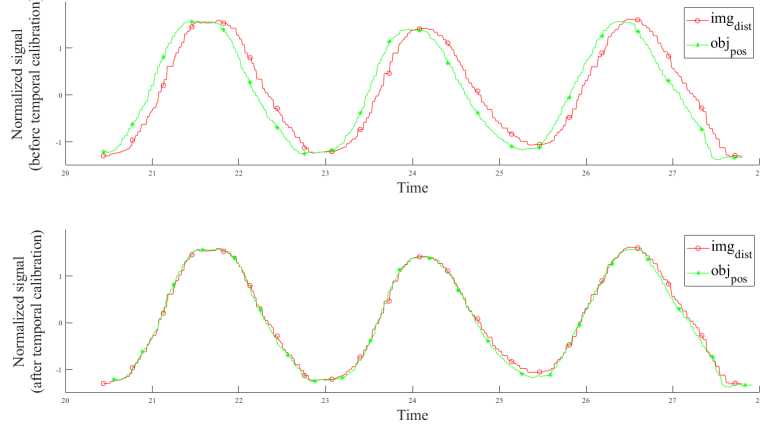


Figure 4: Normalized signals, derived from the tracker position of the line-object and its reflection in the ultrasound image, before and after temporal calibration is applied.

### 3.2 Validation

For initial validation, a qualitative assessment was performed. The 2.5D images were reconstructed from the 2D images obtained from the screen capture of the Conavi console. Transformations were applied to a virtual needle model and the reconstructed volume. Figure 5 shows the needle passing through the needle reflection or point fiducial seen in the image, providing preliminary validation of the calibration method.

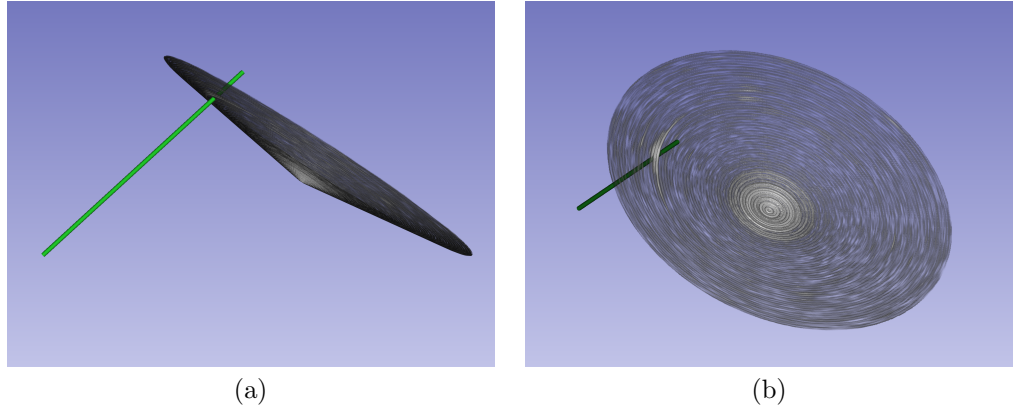


Figure 5: Qualitative validation of calibration method in virtual space. Needle passing through the reconstructed 2.5D ICE image: (a) side view, and (b) top view.

#### 3.2.1 Calibration Precision

Spatial calibration of Foresight ICE probe with a unique 2.5D image was repeated at 5 different angles to observe the translation, rotation and scaling factors of the calibration. Table 1 shows the precision of different parameters of spatial calibration.

$\phi$	$t_x$	$t_y$ (mm)	$t_z$	$r_x$	$r_y$ (°)	$r_z$	$s_x$	$s_y$ (mm/pixel)	$s_z$
85°	-2.68	-1.02	6.22	-0.20	-0.01	2.56	0.16	0.16	0.59
80°	-2.85	0.18	8.87	-0.34	0.28	2.56	0.16	0.17	0.16
75°	-2.26	-1.00	0.54	-0.30	-0.12	2.36	0.16	0.15	0.30
70°	-0.74	-0.51	9.92	-0.28	-0.19	2.43	0.15	0.14	0.25
65°	-4.77	0.19	8.33	-0.03	-0.29	2.35	0.17	0.17	0.11
Mean	-2.66	-0.43	6.78	-0.23	-0.07	2.45	0.16	0.16	0.28
RMS	1.29	0.54	3.34	0.11	0.20	0.09	0.01	0.01	0.17
±95%	±1.13	±0.47	±2.93	±0.09	±0.17	±0.08	±0.01	±0.01	±0.15

Table 1: Precision of spatial calibrations performed at different imaging angles. The overall mean, root mean square (rms) error and 95% confidence interval is given for estimated spatial calibration parameters: translations ( $t_x, t_y, t_z$ ), Euler rotations ( $r_x, r_y, r_z$ ) and scaling factors ( $s_x, s_y, s_z$ )

We observe high variations along z-axis with root-mean-square error in translation ( $t_z$ ) going as high as 3.30 mm. This behavior was expected for two reasons. First, the imaging angle  $\phi$  changes along the z-axis and there may be up to 5° of uncertainty between the imaging angle displayed on the screen and the true physical angle of the conical image in 3D space. Second, the calibration is performed using 3D reconstruction of the 2D screen-capture of the ultrasound image based on the imaging angle  $\phi$ . This reconstruction is prone to some error because of possible data loss from projecting a 2.5D image to a 2D console screen and then reconstruction back to 3D space.

A non-tracked Foresight ICE probe was held still in place while a wooden line was moved to reflect sinusoidally in a 2.5D image plane and generate sensor position  $obj_{pos}$  and reflection position  $img_{dist}$  signals. The experiment was repeated at 3 different angles with at least 5 measurements at each angle. Every measurement includes a minimum of two sinusoidal motion cycles. Results are summarized in Table 2.

$\phi$	Mean temporal offset (ms)	Standard deviation (ms)
85°	98.6	±12.8
75°	86.7	±16.9
65°	93.7	±21.6

Table 2: Precision of temporal calibrations performed multiple times at different imaging angles

An overall mean temporal offset of 93 ms was observed. While a 93 ms offset may account for an appreciable portion of a patient’s cardiac cycle (particularly at higher heart rates), this time delay does not make a perceptible difference in a clinical setting for most applications such as ablation therapies and visualization. However for some applications involving rigorously moving structures, such as segmentation of mitral valve leaflets, this time offset may cause errors. Therefore, for general purposes it is not crucial to correct for temporal offset but some interventions might require it to achieve higher accuracy.

### 3.2.2 Point Source Localization

The cross-wire phantom was secured firmly in a water bath and imaged using a freehand technique. The intersection of the wires, considered as a point source, was imaged from all 4 crossing angles to have a better estimate and reduce bias. B-scan images of the point source are acquired at 15 different positions. Points were manually segmented and converted to the reference coordinate system defined by the CT image volume. All the points were compared to the ground truth defined by the CT of the phantom. Standard error and 95% confidence limit for point reconstruction accuracy is given in Table 3.

### 3.2.3 Spherical Phantom Centroid

The spherical phantom was scanned freehand from different sides. 20 images were acquired and almost ten points along the outline of the sphere were identified in each image. These points were randomly rearranged into 30 groups to enable unbiased distribution of points along the surface of sphere in each measurement. After reconstruction to 3D space, sphere-fitting and coordinate system conversion, the centroids were computed from each group of points and compared to the centroid defined by the CT coordinate system. Using the points on the surface of the sphere, we can also compute accuracy for radial distance and volume measurement, however they were deemed unreliable due to low ultrasound image quality. Table 3 summarizes the results for locating a sphere centroid in a 2.5D ultrasound image.

Validation method	Mean error (mm)			95% Confidence interval (mm)		
	x	y	z	x	y	z
Point source localization	5.07	5.0	4.2	$\pm 2.62$	$\pm 2.58$	$\pm 2.16$
Sphere centroid localization	1.75	0.91	1.94	$\pm 0.64$	$\pm 0.343$	$\pm 0.7$

Table 3: Accuracy of calibrated and tracked Foresight ICE probe described in terms of mean standard error and 95% confidence limits for point source localization and sphere location estimation.

## 4. DISCUSSION

In this work, a calibration method for the unique 2.5D cone-geometry images acquired using a single-element, mechanically scanning intracardiac ultrasound probe was presented and evaluated. Qualitative analysis in a virtual environment shows that the needle intersects with the point fiducial in the 2.5D conical images after calibration. The FRE of the calibration was 1.74 mm in the initial study. However FRE alone does not accurately depict the overall efficacy of a tracking and calibration system. We quantify both the calibration methods and our overall tracking system. We perform point source localization to compute the target registration error (TRE) of the system. Results indicate mean standard error up to 5.07 mm. The 2.5D ultrasound images generated by a single-element mechanically scanning probe is a relatively new concept, and calibration accuracy may be improved once the image generation, acquisition and processing are better understood. Attaching a sensor on the outer sheath of the ultrasound probe also introduces errors in this tracking system. Ideally, the sensor will be integrated rigidly inside the probe, close to the transducer and does not cause any magnetic interference. One major source of error is the large beam profile associated with the single-element transducer. The ultrasound beam is narrow in the center of the image, or near the apex of the cone, and becomes wider at greater depths. With a wider beam, a point source does not appear as a single bright spot in the image but instead as a blurry and spread out ellipsoid and it becomes difficult to define a specific point in the image. Blurring may also be observed as a result of mechanical scanning rotations in the ultrasound probe. These reasons can cause large target localization error which introduces errors in our system accuracy assessment. Beam profile is an inherent property of ultrasound and cannot be improved by the design of an image guidance system. Another source of error, which can potentially be improved as well, is the interchange of coordinate systems. The ultrasound image is generated in 3D space in spherical coordinates, projected on to a 2D screen and then reconstructed back to a 3D Cartesian coordinate system by our system. System accuracy can be improved if these conversions are avoided or performed more efficiently. In spite of these effects potentially causing errors in the system, with the mean error for point source localization appearing to be large, this calibration method may still yield acceptable accuracies, with literature suggesting that for most intracardiac interventions accuracy in the order of 5 mm is required.<sup>13</sup>

We also performed an experiment to image the surface of a sphere and compute its centroid. The results indicate much smaller errors in localization of the centroid of the sphere. We suspect that this behavior is observed because some of the sources of error, such as beam profile and image reconstruction, are biased in a

certain direction. Collecting points, distributed all over the surface, reduces the overall bias by negation and the centroid computed based on multiple, distributed points is more accurate.

It must be noted that the frame-grabber transmitting ultrasound images, and the magnetic tracking system inherently transmit data at different frame-rates. However, we use PLUS library to acquire data from both channels and the time stamps are applied by the PC. PLUS library module estimates and synchronizes the data for the user, thus recording data from both the channels at same time instances. It is not possible for the user to control this data acquisition protocol with PLUS library. The data we collect appears to be intrinsically synchronized, i.e., both the tracker and image data are acquired at the time instant, but in reality this is not completely accurate. That being said, the approximations made by the PLUS library are close enough in time that they do not cause any errors of significance in our workflow and can be assumed correct.

Furthermore, these timestamps are not evenly spaced. In temporal calibration, the correlation is computed between  $img_{dist}$  and copies of  $obj_{pos}$  signal B shifted by a certain number of samples. The temporal offset is given by the number of samples to be delayed in order to achieve maximum correlation between  $img_{dist}$  and  $obj_{pos}$  signals. Since the sampling interval of the magnetic tracking system is not constant throughout the signal, the temporal offset estimation from the number of samples is not factual. These differences however are in the order of a few milliseconds at maximum and can be neglected as they do not make a difference in practice.

System accuracy is directly affected by the uncertainty in the imaging angle  $\phi$ . The probe calibration and tracking method is greatly affected as it is based on the imaging angle displayed on the screen. Small errors in the displayed approximate imaging angle can cause noticeable deviations in the system. While the error may be small near the apex of the cone, it increases as moving towards the distal end of the image. Our future work includes quantifying the imaging angle using a phantom, studying the effect of beam profile on accuracy, and demonstrate an application of tracked single-element ultrasound in intracardiac interventions.

## 5. CONCLUSION

Intracardiac ultrasound probes and their tracking is a vital part of interventional cardiology and cardiac surgery. The accuracy of such a tracking system is dependent on the quality of ultrasound calibration. We describe and validate methods that work for the spatial and temporal calibration of unique 2.5D cone shaped images acquired using Conavi's Foresight ICE system. We use needle or line based methods for both spatial and temporal calibration. Our workflow enables tracking of the ICE probe with the ability to locate a point with the accuracy of 5 mm. The TRE for our system appears to be higher than most calibration methods for planar ultrasound images, primarily because of the large beam profile associated with the single-element ultrasound transducer used in this study. Moreover the unique 2.5D configuration of the image introduce errors when generating a B-scan image at an angle  $\phi$  and when projecting on 2D screen. Even with these limitations, the accuracy of the Conavi Foresight ICE tracking system is still more than acceptable for the image guidance system to be used in a clinical settings to perform intracardiac interventions.

## ACKNOWLEDGMENTS

The authors would like to thank Davidson Ly for help in computer assisted design and 3D printing of our validation phantom

## REFERENCES

- [1] Jongbloed, M. R. M., Schalij, M. J., Zeppenfeld, K., Oemrawsingh, P. V., van der Wall, E. E., and Bax, J. J., "Clinical applications of intracardiac echocardiography in interventional procedures," *Heart (British Cardiac Society)* **91**, 981–90 (jul 2005).
- [2] Courtney, B. and Witcomb, N., "Data display and processing algorithms for 3D imaging systems," (2017).
- [3] Mercier, L., Langø, T., Lindseth, F., and Collins, D. L., "A review of calibration techniques for freehand 3-D ultrasound systems," *Ultrasound in Medicine & Biology* **31**, 449–471 (apr 2005).

- [4] Linte, C. A., Rettmann, M. E., Dilger, B., Gunawan, M. S., Arunachalam, S. P., Holmes, D. R., Packer, D. L., and Robb, R. A., "Calibration and Evaluation of a Magnetically Tracked ICE Probe for Guidance of Left Atrial Ablation Therapy," *Proceedings of SPIE—the International Society for Optical Engineering* **8316**, 83162P (feb 2012).
- [5] "Medical Aurora - Medical." <https://www.ndigital.com/medical/products/aurora/>.
- [6] Lasso, A., Heffter, T., Rankin, A., Pinter, C., Ungi, T., and Fichtinger, G., "PLUS: Open-Source Toolkit for Ultrasound-Guided Intervention Systems," *IEEE Transactions on Biomedical Engineering* **61**, 2527–2537 (oct 2014).
- [7] Fedorov, A., Beichel, R., Kalpathy-Cramer, J., Finet, J., Fillion-Robin, J.-C., Pujol, S., Bauer, C., Jennings, D., Fennessy, F., Sonka, M., Buatti, J., Aylward, S., Miller, J. V., Pieper, S., and Kikinis, R., "3D Slicer as an image computing platform for the Quantitative Imaging Network," *Magnetic resonance imaging* **30**, 1323–41 (nov 2012).
- [8] Chen, E. C. S., Peters, T. M., and Ma, B., "Which point-line registration?," in [*Proc. SPIE 10135, Medical Imaging 2017: Image-Guided Procedures, Robotic Interventions, and Modeling, 1013509*], Webster, R. J. and Fei, B., eds., 1013509 (mar 2017).
- [9] Gobbi, D. G., *Brain deformation correction using interactive 3D ultrasound imaging*, PhD thesis, University of Western Ontario (2003).
- [10] Chen, E. C. S., Peters, T. M., and Ma, B., "Guided ultrasound calibration: where, how, and how many calibration fiducials," *International Journal of Computer Assisted Radiology and Surgery* **11**, 889–898 (jun 2016).
- [11] "Aurora tools and sensors, and accessories." <https://www.ndigital.com/medical/products/tools-and-sensors/>.
- [12] Wold, S., Esbensen, K., and Geladi, P., "Principal component analysis," *Chemometrics and Intelligent Laboratory Systems* **2**(1), 37 – 52 (1987). Proceedings of the Multivariate Statistical Workshop for Geologists and Geochemists.
- [13] Linte, C. A., Moore, J., and Peters, T. M., "How accurate is accurate enough? A brief overview on accuracy considerations in image-guided cardiac interventions," in [*2010 Annual International Conference of the IEEE Engineering in Medicine and Biology*], 2313–2316, IEEE (aug 2010).